10.1098/rspa.2001.0875

THE ROYAL SOCIETY

# Mindlin's problem for an anisotropic piezoelectric half-space with general boundary conditions

By E. Pan

*Structures Technology, Inc., 543 Keisler Drive, Suite 204, Cary, NC 27511, USA* (ernian_pan@yahoo.com)

*Received 26 March 2001; accepted 2 July 2001; published online 29 November 2001*

This paper considers Mindlin's problem in an anisotropic and piezoelectric half-space with general boundary conditions, including 16 different sets of surface conditions. The Green's function due to a point force or point electric charge within the half-space, also called the generalized Mindlin problem, is solved. Based on the extended Stroh formalism and two-dimensional Fourier transforms in combination with Mindlin's superposition method, the generalized Mindlin solution is expressed as a sum of the generalized Kelvin solution and a complementary part. While the full-space Green's function is in an explicit form, the complementary part is expressed in terms of a simple line integral over $[0, \pi]$. Of the 16 different sets, detailed studies are presented for the four common surface conditions, i.e. the traction-free insulating and conducting, and rigid insulating and conducting surface conditions. With the exception of the solution to the traction-free insulating boundary condition, solutions to the other sets of boundary conditions are new. Furthermore, the corresponding two-dimensional solutions are also derived analytically for the 16 different sets of boundary conditions for possibly the first time.

Numerical examples of the generalized Mindlin solution are carried out for two typical piezoelectric materials, one being quartz and the other ceramic, with the four common surface conditions. These numerical results illustrate clearly the significance of different boundary conditions as well as the electromechanical coupling in the Mindlin's problem analysis.

**Keywords: Mindlin's problem; piezoelectric material; Green's function; Stroh formalism; general boundary condition; strained quantum devices**

## 1. Introduction

Green's functions (i.e. the fundamental solutions due to a concentrated source) are of great importance in various engineering and physical fields. In linear elasticity, various two-dimensional (2D) and three-dimensional (3D) Green's functions have been derived so far (Bacon *et al.* 1978; Mura 1987; Ting 1996, 2000). While most 2D elastic Green's functions can be found in the book by Ting (1996), a brief review on the 3D Green's functions in an elastic full-space and bimaterials can be found in a recent paper by the author (Pan 2002*b*), where the Green's function in an anisotropic elastic half-space with general boundary conditions was derived. Besides the purely elastic Green's functions, some fully coupled piezoelectric Green's functions have also

 

been derived and applied to the analysis of micromechanical devices and composite structures (Suo *et al.* 1992; Dunn & Taya 1993; Ting 1996). More interestingly, certain generalized Hertzian contact problems (Willis 1966) were also studied based on the fully coupled piezoelectric Green's functions (Fan *et al.* 1996; Chen 1999; Chen *et al.* 1999).

In recent years, Green's functions (3D Green's functions in particular) and the related analytical methods have been found to be particularly useful in the study of the strained semiconductor quantum devices where the strain-induced quantum dot growth in semiconductor nanostructures is crucial to the electronic performance (see, for example, Andreev *et al.* 1999; Davies 1998; Davies & Larkin 1994; Faux & Pearson 2000; Faux *et al.* 1996, 1997; Freund 2000; Freund & Gosling 1995; Gosling & Willis 1995; Larkin *et al.* 1997; Holy *et al.* 1999; Park & Chuang 1998; Pearson & Faux 2000). Even though certain analytical results obtained so far have shed some light on explaining the orientation and ordering of the quantum dot growth (Holy *et al.* 1999; Faux & Pearson 2000), almost all available models are based on either the uncoupled purely elastic model or simplified semi-coupled models. The fully coupled electromechanical problem has not been considered so far, with the exception of the 2D deformation, where Ru (1999, 2000, 2001) solved Eshelby's problem in a piezoelectric infinite plane, a half-plane, and bimaterial planes with fully coupled constitutive relation. Furthermore, Ru's (2001) closed-form solution for the half-plane case has clearly indicated the effect of different piezoelectric boundary conditions on the surface response of both mechanical and electric quantities. Therefore, under 3D deformation, the fully coupled piezoelectric 3D Green's functions, as embedded in the Eshelby tensor (Eshelby 1957; Mura 1987), should be employed in the reliable analysis of the strained quantum dot growth. In particular, the 3D Green's functions in a fully coupled piezoelectric half-space under various surface boundary conditions, or the generalized Mindlin solutions, are of special values in the modelling of the strain-induced quantum dot growth.

Due to the complicated electromechanical coupling, however, only a few types of Green's functions have been developed so far for the fully coupled piezoelectric case under 3D deformation. For the case of transversely isotropic piezoelectric materials, the Green's functions in an infinite space, a half-space, and bimaterials were obtained by Dunn & Wienecke (1996, 1999) and Ding *et al.* (1997, 1999). For a general anisotropic piezoelectric infinite space, while Akamatsu & Tanuma (1997) derived the Green's elastic displacement and electric potential, Pan & Tonon (2000) proposed a method for the calculation of the complete Green's function components. Based on the generalized Stroh formulism (Ting 1996) and Mindlin's superposition method (Mindlin 1936), Pan & Yuan (2000) recently derived the 3D Green's functions in a general anisotropic piezoelectric half-space and bimaterials. However, with the exception of the traction-free insulating surface where the generalized Mindlin solutions for the transversely isotropic (Dunn & Wienecke 1996, 1999; Ding *et al.* 1997, 1999) and general anisotropic (Pan & Yuan 2000) half-spaces are available, no other generalized Mindlin solutions exist in the literature for a general anisotropic piezoelectric half-space with other surface conditions.

This paper solves the Mindlin's problem in an anisotropic and piezoelectric half-space, or the generalized Mindlin function with general boundary conditions on the surface of the half-space. In total, 16 different sets of boundary conditions are solved, including the four common boundary conditions, namely, traction-free insulating

and conducting, and rigid insulating and conducting conditions (Ru 2001). The generalized Mindlin solution is derived based on the extended Stroh formalism and 2D Fourier transforms in combination with Mindlin's superposition method, and is expressed as a sum of the generalized Kelvin solution and a complementary part. While the former is in an explicit form, as previously derived by Pan & Tonon (2000), the complementary part is expressed in terms of a simple line integral over $[0, \pi]$. Of the 16 different sets, only the solution to the traction-free insulating surface was solved before (Pan & Yuan 2000); solutions to the other 15 sets of boundary conditions are presented in this paper for possibly the first time. Furthermore, under the assumption of 2D deformation, solutions to the 16 different sets of boundary conditions are also derived analytically (without any line integral).

Based on the generalized Mindlin solution, the effect of different surface conditions on the elastic and electric quantities is then studied and discussed for the four common surface conditions. To illustrate the significance of different boundary conditions as well as the electromechanical coupling in piezoelectric problem analysis, numerical examples are carried out for two typical piezoelectric materials, namely, the quartz with weak coupling and ceramic with strong coupling. It is found that, if the point source is mechanical (electric), then the corresponding mechanical (electric) response on the surface of the half-space is nearly independent of the electric (mechanical) boundary conditions for the quartz. In other words, for these cases, the corresponding uncoupled purely elastic (electric) model could be employed to avoid the complexity due to the coupling. However, owing to its high degree of electromechanical coupling for the ceramic, the uncoupled purely elastic (electric) model is only applicable for certain quantities in the vicinity of the surface point above the source and therefore should be adopted with extreme caution. On the other hand, if one is also interested in the mechanical (electric) response on the surface of the half-space due to an electric (mechanical) point source, then the four different sets of boundary conditions can all significantly affect the surface response and the coupled (preferably the fully coupled) piezoelectric model needs to be used, even if the electromechanical coupling is weak.

It is believed that the generalized Mindlin solution should be useful for the study of various modern devices, in particular of the strained semiconductor quantum devices. This solution is also of interest in the corresponding 3D Eshelby problem in composite materials and in various integral equation approaches based on the Green's function method.

This paper is organized as follows. In § 2, the generalized Mindlin problem is defined along with the mathematical equations. In § 3, the Stroh formalism and the general solution in the Fourier-transformed domain are given. While in § 4 the generalized Mindlin solution is derived, the effect of different surface boundary conditions on the elastic and electric fields is studied in § 5. Numerical examples are presented in § 6, and certain conclusions are drawn in § 7. Throughout this paper, by generalized Mindlin solutions, or Green's functions, we mean the elastic displacements and electric potential, elastic stresses and electric displacements, and derivatives of them with respect to the source coordinates.

## 2. Description of the generalized Mindlin problem

Similar to the classical Mindlin problem (Mindlin 1936), we consider in this paper the static deformation of a linearly anisotropic piezoelectric half-space occupying the

domain $x_3 > 0$ bounded by the flat surface plane $x_3 = 0$. While the surface is under general boundary conditions (to be defined later), a concentrated force or electric charge is applied at a point source within the half-space. The governing equations consist of the following (see, for example, Tiersten 1969; Barnett & Lothe 1975; Pan 1999).

*Equilibrium equations*

$$\sigma_{ji,j} + f_i = 0; \qquad D_{i,i} - q = 0, \tag{2.1}$$

where $\sigma_{ij}$ and $D_i$ are the stress and electric displacement, respectively; $f_i$ and $q$ are the body force and electric charge density, which will be replaced later by a concentrated force and electric charge. In this paper, lowercase (uppercase) subscripts always range from 1 to 3 (1 to 4) and summation over repeated lowercase (uppercase) subscripts is implied. A subscript comma denotes the partial differentiation with respect to the coordinates (i.e. $x_1$, $x_2$, $x_3$ or $x$, $y$, $z$).

*Constitutive relations*

$$\sigma_{ij} = C_{ijlm}\gamma_{lm} - e_{kji}E_k, \qquad D_i = e_{ijk}\gamma_{jk} + \varepsilon_{ij}E_j, \tag{2.2}$$

where $\gamma_{ij}$ is the strain and $E_i$ is the electric field; $C_{ijlm}$, $e_{ijk}$ and $\varepsilon_{ij}$ are the elastic moduli, the piezoelectric coefficients, and the dielectric constants, respectively. It is required that these coefficients satisfy the well-known symmetry conditions (Pan 1999). The decoupled state (purely elastic and purely electric deformations) can be obtained by simply setting $e_{ijk} = 0$, one of the procedures adopted in almost all previous studies in strained quantum devices. Another procedure is to use the semi-coupled model where the first constitutive relation of (2.2) is used to solve the purely elastic field by dropping the second term on the right-hand side (i.e. $e_{ijk} = 0$), and the second relation of (2.2) is then used to estimate the electric field induced by the purely elastic field (i.e. elastic strain with $e_{ijk} \neq 0$). One should be very cautious when using these decoupled or semi-coupled models, since substantial errors may be introduced, as will be illustrated numerically later.

*Elastic strain-displacement and electric field-potential relations*

$$\gamma_{ij} = \tfrac{1}{2}(u_{i,j} + u_{j,i}); \qquad E_i = -\phi_{,i}, \tag{2.3}$$

where $u_i$ and $\phi$ are the elastic displacement and electric potential, respectively.

The notation introduced by Barnett & Lothe (1975) has been shown to be very convenient for the analysis of piezoelectric problems. With this notation, the elastic displacement and electric potential, the elastic strain and electric field, the stress and electric displacement, and the elastic and electric moduli (or coefficients) can be grouped together as (Barnett & Lothe 1975; Dunn & Taya 1993; Pan 1999):

$$u_I = \begin{cases} u_i, & I = 1, 2, 3, \\ \phi, & I = 4, \end{cases} \tag{2.4}$$

$$\gamma_{Ij} = \begin{cases} \gamma_{ij}, & I = 1, 2, 3, \\ -E_j, & I = 4, \end{cases} \tag{2.5}$$

$$\sigma_{iJ} = \begin{cases} \sigma_{ij}, & J = 1, 2, 3, \\ D_i, & J = 4, \end{cases} \tag{2.6}$$

$$C_{iJKl} = \begin{cases} C_{ijkl}, & J, K = 1, 2, 3, \\ e_{lij}, & J = 1, 2, 3, \ K = 4, \\ e_{ikl}, & J = 4, \ K = 1, 2, 3, \\ -\varepsilon_{il}, & J = K = 4. \end{cases} \tag{2.7}$$

In terms of this shorthand notation, the constitutive relations (2.2) can be unified into the single equation:

$$\sigma_{iJ} = C_{iJKl}\gamma_{Kl}. \tag{2.8}$$

Similarly, the equilibrium equations (2.1) in terms of *the extended stresses* can be recast into

$$\sigma_{iJ,i} + f_J = 0 \tag{2.9}$$

with $f_J$ being defined as

$$f_J = \begin{cases} f_j, & J = 1, 2, 3, \\ -q, & J = 4. \end{cases} \tag{2.10}$$

For ease of reference, we will occasionally, in the following sections, use *the extended displacement* for the elastic displacement and electric potential as defined by (2.4), and *the extended stress* for the stress and electric displacement as defined by (2.6).

Following Pan (2002*b*), we write the general boundary condition on the surface of the half-space by a simple vector equation that is similar to the purely elastic counterpart,

$$\boldsymbol{I}_u\boldsymbol{u} + \boldsymbol{I}_t\boldsymbol{t} = \boldsymbol{0}, \tag{2.11}$$

where $\boldsymbol{I}_u$ and $\boldsymbol{I}_t$ are $4 \times 4$ diagonal matrices whose four diagonal elements are either one or zero, and satisfy conditions

$$\boldsymbol{I}_u + \boldsymbol{I}_t = \boldsymbol{I}; \qquad \boldsymbol{I}_u\boldsymbol{I}_t = \boldsymbol{0} \tag{2.12}$$

with $\boldsymbol{I}$ being the unit matrix, and

$$\boldsymbol{t} = (\sigma_{31}, \sigma_{32}, \sigma_{33}, D_3) \tag{2.13}$$

is the *extended traction* on the $z = \text{const.}$ plane.

Equation (2.11) includes a total of 16 different boundary condition sets, of which the following six sets are particularly interesting:

$$\left.\begin{array}{cccc} t_1 = 0, & t_2 = 0, & t_3 = 0, & t_4 = 0, \\ t_1 = 0, & t_2 = 0, & t_3 = 0, & u_4 = 0, \\ u_1 = 0, & u_2 = 0, & u_3 = 0, & t_4 = 0, \\ u_1 = 0, & u_2 = 0, & u_3 = 0, & u_4 = 0, \\ t_1 = 0, & t_2 = 0, & u_3 = 0, & t_4 = 0, \\ t_1 = 0, & t_2 = 0, & u_3 = 0, & u_4 = 0. \end{array}\right\} \tag{2.14}$$

Table 1. *The six sets of piezoelectric boundary conditions (BCs)*

| name of the BC | mechanical BC | electric BC |
|---|---|---|
| traction-free insulating | $\sigma_{31} = \sigma_{32} = \sigma_{33} = 0$ | $D_3 = 0$ |
| traction-free conducting | $\sigma_{31} = \sigma_{32} = \sigma_{33} = 0$ | $\phi = 0$ |
| rigid insulating | $u_1 = u_2 = u_3 = 0$ | $D_3 = 0$ |
| rigid conducting | $u_1 = u_2 = u_3 = 0$ | $\phi = 0$ |
| slippery insulating | $\sigma_{31} = \sigma_{32} = 0$; $u_3 = 0$ | $D_3 = 0$ |
| slippery conducting | $\sigma_{31} = \sigma_{32} = 0$; $u_3 = 0$ | $\phi = 0$ |

For these boundary conditions, the diagonal matrices $\boldsymbol{I}_u$ and $\boldsymbol{I}_t$ take the following diagonal elements:

$$\left.\begin{aligned} \boldsymbol{I}_u &= \operatorname{diag}[0,0,0,0], \quad \boldsymbol{I}_t = \operatorname{diag}[1,1,1,1],\\ \boldsymbol{I}_u &= \operatorname{diag}[0,0,0,1], \quad \boldsymbol{I}_t = \operatorname{diag}[1,1,1,0],\\ \boldsymbol{I}_u &= \operatorname{diag}[1,1,1,0], \quad \boldsymbol{I}_t = \operatorname{diag}[0,0,0,1],\\ \boldsymbol{I}_u &= \operatorname{diag}[1,1,1,1], \quad \boldsymbol{I}_t = \operatorname{diag}[0,0,0,0],\\ \boldsymbol{I}_u &= \operatorname{diag}[0,0,1,0], \quad \boldsymbol{I}_t = \operatorname{diag}[1,1,0,1],\\ \boldsymbol{I}_u &= \operatorname{diag}[0,0,1,1], \quad \boldsymbol{I}_t = \operatorname{diag}[1,1,0,0]. \end{aligned}\right\} \tag{2.15}$$

It is apparent that the first and second sets of (2.14) correspond to the traction-free insulating and traction-free conducting conditions, respectively; the third and fourth sets to the rigid insulating and rigid conducting conditions, respectively; and the fifth and sixth sets to the slippery insulating and slippery conducting conditions, respectively. To show a clear connection between the name of the boundary condition and the physical quantities involved, these six sets of boundary conditions are further listed in table 1.

We now let an extended point force $\boldsymbol{f} = (f_1, f_2, f_3, f_4)$ be applied in the half-space at the source point $\boldsymbol{d} \equiv (d_1, d_2, d_3 \equiv d)$ with $d_3 > 0$ and the field point be denoted by $\boldsymbol{x} \equiv (x_1, x_2, x_3 \equiv z)$.† To solve the homogeneous counterpart of (2.9), we artificially divide the problem domain into two regions: $z > d$ and $0 \leqslant z < d$. While these two regions are free of body force and electric charge, at their artificial interface $z = d$, where the extended point source is applied, the extended displacement and traction vectors are required to satisfy the following conditions

$$\left.\begin{aligned} \boldsymbol{u}|_{z=d^-} &= \boldsymbol{u}|_{z=d^+},\\ \boldsymbol{t}|_{z=d^-} - \boldsymbol{t}|_{z=d^+} &= \delta(x_1 - d_1)\delta(x_2 - d_2)\boldsymbol{f}. \end{aligned}\right\} \tag{2.16}$$

Therefore, in summary, the generalized Mindlin's problem is to find the elastic and electric fields that satisfy (2.9) with $\boldsymbol{f} = \boldsymbol{0}$ for the two regions $z > d$ and $0 \leqslant z < d$, the general boundary condition (2.11), the conditions (2.16) at the source level, along with the condition that the solution in the half-space is bounded as $|\boldsymbol{x}|$ approaches infinity.

† Thereafter, the scalar variables $z$ and $d$ will be used exclusively for the third field coordinate $x_3$ and the third source coordinate $d_3$, respectively.

## 3. Stroh formalism and solution in the transformed domain

Similar to the corresponding purely elastic counterpart, we will first apply the two-dimensional Fourier transforms to the problem equations and then express the Fourier transformed solutions in terms of the extended Stroh formalism (Ting 1996; Pan & Yuan 2000). The procedure is briefly described below.

First, the 2D Fourier transforms (i.e. for the two-point extended displacement)

$$\tilde{u}_K(y_1, y_2, z; \boldsymbol{d}) = \iint u_K(x_1, x_2, z; \boldsymbol{d}) \mathrm{e}^{\mathrm{i}y_\alpha x_\alpha} \, \mathrm{d}x_1 \mathrm{d}x_2 \tag{3.1}$$

are applied to (2.8) and (2.9). In (3.1), $\alpha$ takes the summation from 1 to 2.

A general solution to the Fourier transformed equations of (2.8) and (2.9) in terms of the extended displacement can be derived as (Pan & Yuan 2000)

$$\tilde{\boldsymbol{u}}(y_1, y_2, z; \boldsymbol{d}) = \boldsymbol{a} \mathrm{e}^{-\mathrm{i}p\eta z} \tag{3.2}$$

with $p$ and $\boldsymbol{a}$ satisfying the following eigenrelation:

$$[\boldsymbol{Q} + p(\boldsymbol{R} + \boldsymbol{R}^{\mathrm{T}}) + p^2 \boldsymbol{T}]\boldsymbol{a} = 0, \tag{3.3}$$

where the superscript 'T' denotes matrix transpose, and

$$Q_{IK} = C_{jIKs} n_j n_s, \qquad R_{IK} = C_{jIKs} n_j m_s, \qquad T_{IK} = C_{jIKs} m_j m_s \tag{3.4}$$

with

$$\left.\begin{aligned} (n_1, n_2, n_3) &\equiv (\cos\theta, \sin\theta, 0), \\ (m_1, m_2, m_3) &\equiv (0, 0, 1). \end{aligned}\right\} \tag{3.5}$$

Note that a polar coordinate transform, defined below, has been used:

$$y_1 = \eta \cos\theta; \qquad y_2 = \eta \sin\theta. \tag{3.6}$$

Equation (3.3) is the Stroh eigenrelation for the oblique plane spanned by $\boldsymbol{n}$ and $\boldsymbol{m}$ defined by (3.5). By the positive requirement on the strain energy density, it can be shown (see, for example, Ting 1996) that its eigenvalues are either complex or purely imaginary.

Second, using the Stroh eigenvalues and eigenvectors, the extended traction vector $\boldsymbol{t}$ on the $z =$ const. plane, and the in-plane stress vector $\boldsymbol{s}$, defined as

$$\boldsymbol{s} = (\sigma_{11}, \sigma_{12}, \sigma_{22}, D_1, D_2) \tag{3.7}$$

can be derived in the Fourier-transformed domain as (Pan & Yuan 2000)

$$\tilde{\boldsymbol{t}} = -\mathrm{i}\eta \boldsymbol{b} \mathrm{e}^{-\mathrm{i}p\eta z}, \tag{3.8}$$

$$\tilde{\boldsymbol{s}} = -\mathrm{i}\eta \boldsymbol{c} \mathrm{e}^{-\mathrm{i}p\eta z}, \tag{3.9}$$

with

$$\left.\begin{aligned} \boldsymbol{b} &= (\boldsymbol{R}^{\mathrm{T}} + p\boldsymbol{T})\boldsymbol{a} = -\frac{1}{p}(\boldsymbol{Q} + p\boldsymbol{R})\boldsymbol{a}, \\ \boldsymbol{c} &= \boldsymbol{H}\boldsymbol{a}, \end{aligned}\right\} \tag{3.10}$$

where the matrix $\boldsymbol{H}$ is defined by

$$\begin{bmatrix} C_{111\alpha}n_\alpha + pC_{1113} & C_{112\alpha}n_\alpha + pC_{1123} & C_{113\alpha}n_\alpha + pC_{1133} & C_{114\alpha}n_\alpha + pC_{1143} \\ C_{121\alpha}n_\alpha + pC_{1213} & C_{122\alpha}n_\alpha + pC_{1223} & C_{123\alpha}n_\alpha + pC_{1233} & C_{124\alpha}n_\alpha + pC_{1243} \\ C_{221\alpha}n_\alpha + pC_{2213} & C_{222\alpha}n_\alpha + pC_{2223} & C_{223\alpha}n_\alpha + pC_{2233} & C_{224\alpha}n_\alpha + pC_{2243} \\ C_{141\alpha}n_\alpha + pC_{1413} & C_{142\alpha}n_\alpha + pC_{1423} & C_{143\alpha}n_\alpha + pC_{1433} & C_{144\alpha}n_\alpha + pC_{1443} \\ C_{241\alpha}n_\alpha + pC_{2413} & C_{242\alpha}n_\alpha + pC_{2423} & C_{243\alpha}n_\alpha + pC_{2433} & C_{244\alpha}n_\alpha + pC_{2443} \end{bmatrix} \tag{3.11}$$

again with $\alpha$ taking the summation from 1 to 2.

Denoting by $p_m$, $\boldsymbol{a}_m$ and $\boldsymbol{b}_m$ $(m = 1, 2, \ldots, 8)$ the eigenvalues and the associated eigenvectors of (3.3), we then order them in such a way so that

$$\left.\begin{aligned} &\operatorname{Im} p_J > 0, \quad p_{J+4} = \bar{p}_J, \quad \boldsymbol{a}_{J+4} = \bar{\boldsymbol{a}}_J, \quad \boldsymbol{b}_{J+4} = \bar{\boldsymbol{b}}_J \quad (J = 1, 2, 3, 4), \\ &\boldsymbol{A} = [\boldsymbol{a}_1, \boldsymbol{a}_2, \boldsymbol{a}_3, \boldsymbol{a}_4], \quad \boldsymbol{B} = [\boldsymbol{b}_1, \boldsymbol{b}_2, \boldsymbol{b}_3, \boldsymbol{b}_4], \quad \boldsymbol{C} = [\boldsymbol{c}_1, \boldsymbol{c}_2, \boldsymbol{c}_3, \boldsymbol{c}_4, \boldsymbol{c}_5], \end{aligned}\right\} \tag{3.12}$$

where Im stands for the imaginary part and overbar for the complex conjugate. In the analysis followed, we assume that $p_J$ are distinct and the eigenvectors $\boldsymbol{a}_J$ and $\boldsymbol{b}_J$ satisfy the normalization relation (Barnett & Lothe 1975; Ting 1996)

$$\boldsymbol{b}_I^{\mathrm{T}}\boldsymbol{a}_J + \boldsymbol{a}_I^{\mathrm{T}}\boldsymbol{b}_J = \delta_{IJ} \tag{3.13}$$

with $\delta_{IJ}$ being the $4\times4$ Kronecker delta, i.e. the $4\times4$ identity matrix. We also remark that repeated eigenvalues $p_J$ can be avoided by using slightly perturbed material coefficients with negligible errors (Pan 1997). In doing so, the simple structure of the solution presented below can always be used.

Finally, the general solutions in the Fourier transformed domain, which satisfy condition (2.16) at the source level and the condition at infinity, can be derived as (Pan & Yuan 2000)

For $0 \leqslant z < d$:

$$\left.\begin{aligned} \tilde{\boldsymbol{u}}(y_1, y_2, z; \boldsymbol{d}) &= \mathrm{i}\eta^{-1}\boldsymbol{A}\langle \mathrm{e}^{-\mathrm{i}p_*\eta(z-d)}\rangle \boldsymbol{q}^\infty - \mathrm{i}\eta^{-1}\bar{\boldsymbol{A}}\langle \mathrm{e}^{-\mathrm{i}\bar{p}_*\eta z}\rangle \boldsymbol{q}, \\ \tilde{\boldsymbol{t}}(y_1, y_2, z; \boldsymbol{d}) &= \boldsymbol{B}\langle \mathrm{e}^{-\mathrm{i}p_*\eta(z-d)}\rangle \boldsymbol{q}^\infty - \bar{\boldsymbol{B}}\langle \mathrm{e}^{-\mathrm{i}\bar{p}_*\eta z}\rangle \boldsymbol{q}, \\ \tilde{\boldsymbol{s}}(y_1, y_2, z; \boldsymbol{d}) &= \boldsymbol{C}\langle \mathrm{e}^{-\mathrm{i}p_*\eta(z-d)}\rangle \boldsymbol{q}^\infty - \bar{\boldsymbol{C}}\langle \mathrm{e}^{-\mathrm{i}\bar{p}_*\eta z}\rangle \boldsymbol{q}. \end{aligned}\right\} \tag{3.14}$$

For $z > d$:

$$\left.\begin{aligned} \tilde{\boldsymbol{u}}(y_1, y_2, z; \boldsymbol{d}) &= -\mathrm{i}\eta^{-1}\bar{\boldsymbol{A}}\langle \mathrm{e}^{-\mathrm{i}\bar{p}_*\eta(z-d)}\rangle \bar{\boldsymbol{q}}^\infty - \mathrm{i}\eta^{-1}\bar{\boldsymbol{A}}\langle \mathrm{e}^{-\mathrm{i}\bar{p}_*\eta z}\rangle \boldsymbol{q}, \\ \tilde{\boldsymbol{t}}(y_1, y_2, z; \boldsymbol{d}) &= -\bar{\boldsymbol{B}}\langle \mathrm{e}^{-\mathrm{i}\bar{p}_*\eta(z-d)}\rangle \bar{\boldsymbol{q}}^\infty - \bar{\boldsymbol{B}}\langle \mathrm{e}^{-\mathrm{i}\bar{p}_*\eta z}\rangle \boldsymbol{q}, \\ \tilde{\boldsymbol{s}}(y_1, y_2, z; \boldsymbol{d}) &= -\bar{\boldsymbol{C}}\langle \mathrm{e}^{-\mathrm{i}\bar{p}_*\eta(z-d)}\rangle \bar{\boldsymbol{q}}^\infty - \bar{\boldsymbol{C}}\langle \mathrm{e}^{-\mathrm{i}\bar{p}_*\eta z}\rangle \boldsymbol{q}, \end{aligned}\right\} \tag{3.15}$$

where

$$\boldsymbol{q}^\infty = \boldsymbol{A}^{\mathrm{T}}\boldsymbol{f}\mathrm{e}^{\mathrm{i}y_\alpha d_\alpha}, \qquad \bar{\boldsymbol{q}}^\infty = \bar{\boldsymbol{A}}^{\mathrm{T}}\boldsymbol{f}\mathrm{e}^{\mathrm{i}y_\alpha d_\alpha} \tag{3.16}$$

and

$$\langle \mathrm{e}^{-\mathrm{i}p_*\eta z}\rangle = \operatorname{diag}\left[\mathrm{e}^{-\mathrm{i}p_1\eta z} \quad \mathrm{e}^{-\mathrm{i}p_2\eta z} \quad \mathrm{e}^{-\mathrm{i}p_3\eta z} \quad \mathrm{e}^{-\mathrm{i}p_4\eta z}\right]. \tag{3.17}$$

The complex vector $\boldsymbol{q}$ in (3.14) and (3.15) is to be determined.

The challenge now is to determine $\boldsymbol{q}$ for the given general boundary conditions (2.11). Fortunately, a procedure similar to the corresponding purely elastic half-space

problem (Pan 2002*b*) can be followed. This is achieved by defining a new complex matrix $\boldsymbol{K}$ of $4 \times 4$ as

$$\boldsymbol{K} = \boldsymbol{I}_u \boldsymbol{A} + \boldsymbol{I}_t \boldsymbol{B} \tag{3.18}$$

a suitable combination of the Stroh eigenmatrices $\boldsymbol{A}$ and $\boldsymbol{B}$ that are properly coupled with the boundary conditions. It is seen that the matrix $\boldsymbol{K}$, like the eigenvalues $p_J$ and the eigenmatrices $\boldsymbol{A}$ and $\boldsymbol{B}$, is independent of the radial variable $\eta$ (but is a function of $\theta$!), an important feature to be used later. For the six sets of boundary conditions (2.14), the matrix $\boldsymbol{K}$ has the following expressions:

$$\boldsymbol{K}_{\rm fi} = \begin{bmatrix} B_{11} & B_{12} & B_{13} & B_{14} \\ B_{21} & B_{22} & B_{23} & B_{24} \\ B_{31} & B_{32} & B_{33} & B_{34} \\ B_{41} & B_{42} & B_{43} & B_{44} \end{bmatrix}, \qquad \boldsymbol{K}_{\rm fc} = \begin{bmatrix} B_{11} & B_{12} & B_{13} & B_{14} \\ B_{21} & B_{22} & B_{23} & B_{24} \\ B_{31} & B_{32} & B_{33} & B_{34} \\ A_{41} & A_{42} & A_{43} & A_{44} \end{bmatrix}, \tag{3.19}$$

$$\boldsymbol{K}_{\rm ri} = \begin{bmatrix} A_{11} & A_{12} & A_{13} & A_{14} \\ A_{21} & A_{22} & A_{23} & A_{24} \\ A_{31} & A_{32} & A_{33} & A_{34} \\ B_{41} & B_{42} & B_{43} & B_{44} \end{bmatrix}, \qquad \boldsymbol{K}_{\rm rc} = \begin{bmatrix} A_{11} & A_{12} & A_{13} & A_{14} \\ A_{21} & A_{22} & A_{23} & A_{24} \\ A_{31} & A_{32} & A_{33} & A_{34} \\ A_{41} & A_{42} & A_{43} & A_{44} \end{bmatrix}, \tag{3.20}$$

$$\boldsymbol{K}_{\rm si} = \begin{bmatrix} B_{11} & B_{12} & B_{13} & B_{14} \\ B_{21} & B_{22} & B_{23} & B_{24} \\ A_{31} & A_{32} & A_{33} & A_{34} \\ B_{41} & B_{42} & B_{43} & B_{44} \end{bmatrix}, \qquad \boldsymbol{K}_{\rm sc} = \begin{bmatrix} B_{11} & B_{12} & B_{13} & B_{14} \\ B_{21} & B_{22} & B_{23} & B_{24} \\ A_{31} & A_{32} & A_{33} & A_{34} \\ A_{41} & A_{42} & A_{43} & A_{44} \end{bmatrix}, \tag{3.21}$$

where two subscripts are introduced to indicate the corresponding boundary conditions with the first one for mechanical and the second for electric conditions. Therefore, the first and second expressions of (3.19) are for the traction-free insulating ('fi') and traction-free conducting ('fc') surfaces, the first and second expressions of (3.20) are for the rigid insulating ('ri') and rigid conducting ('rc') surfaces, and the first and second expressions of (3.21) are for the slippery insulating ('si') and slippery conducting ('sc') surfaces.

With the new matrix $\boldsymbol{K}$, the complex vector $\boldsymbol{q}$ for all the 16 different sets of boundary conditions (2.11) can therefore be expressed in a simple vector equation as

$$\boldsymbol{q} = \bar{\boldsymbol{K}}^{-1} \boldsymbol{K} \langle \mathrm{e}^{\mathrm{i}p_* \eta d} \rangle \boldsymbol{A}^{\mathrm{T}} \boldsymbol{f} \mathrm{e}^{\mathrm{i}y_\alpha d_\alpha}. \tag{3.22}$$

Equation (3.22) is a very surprising result and it will be the key when deriving the physical-domain Green's functions, i.e. the generalized Mindlin solutions.

Before carrying out the inverse transform, we mention several important features associated with the Fourier transformed-domain solutions (3.14) and (3.15).

1. The first terms in (3.14) and (3.15) are the Fourier transformed Green's function for an anisotropic and piezoelectric full-space. Inverse of this Green's function, i.e. the physical-domain solution or the generalized Kelvin solution, has been derived recently by Akamatsu & Tanuma (1997) and Pan & Tonon (2000) in an explicit form. Therefore, the inverse of the Fourier transform needs to be carried out only for the second terms of the solution. This procedure resembles the Mindlin solution method (Mindlin 1936).

2. The unified Fourier transformed solution includes all the 16 different sets of boundary conditions (2.11). Thus, to solve the anisotropic and piezoelectric

half-space problem with different boundary conditions, one only needs to assign the matrix $\boldsymbol{K}$ defined by (3.18) to the corresponding boundary condition, a remarkable concise result.

3. In deriving the Fourier transformed solution, the matrix $\boldsymbol{K}$ has been assumed to be non-singular. This can be proved following a procedure similar to Ting (1996).

## 4. Generalized Mindlin solution

Having obtained the Fourier transformed-domain solution, we now apply the inverse Fourier transform to (3.14) and (3.15). To handle the double infinite integrals, the polar coordinate transform (3.6) is introduced so that the infinite integral with respect to the radial variable $\eta$ can be carried out exactly. Thus, the final half-space Green's function in the physical domain, or the generalized Mindlin solution, can be expressed as a sum of an explicit Kelvin solution and a complementary part in terms of a line integral over $[0, 2\pi]$. Furthermore, the latter can be reduced to an integral over $[0, \pi]$ (Pan 2002*a*, *b*). After some tedious but straightforward manipulations, the generalized Mindlin solution can be expressed in a compact form. For the half-space displacement tensor ($4 \times 4$), with its row and column indices being the component of the field quantity and the direction of the point source, respectively, we found

$$\boldsymbol{U}(\boldsymbol{x}; \boldsymbol{d}) = \boldsymbol{U}^{\infty}(\boldsymbol{x}; \boldsymbol{d}) + \frac{1}{2\pi^2} \int_0^{\pi} \bar{\boldsymbol{A}} \boldsymbol{G}_1 \boldsymbol{A}^{\mathrm{T}} \, \mathrm{d}\theta, \tag{4.1}$$

where†

$$(\boldsymbol{G}_1)_{IJ} = \frac{(\bar{\boldsymbol{K}}^{-1}\boldsymbol{K})_{IJ}}{-\bar{p}_I z + p_J d - [(x_1 - d_1)\cos\theta + (x_2 - d_2)\sin\theta]}. \tag{4.2}$$

The first term in (4.1) corresponds to the Green's displacement tensor, or the generalized Kelvin tensor, in an anisotropic and piezoelectric full-space, which is already available in an explicit form (Akamatsu & Tanuma 1997; Pan & Tonon 2000). Consequently, the half-space displacement tensor can be expressed as a sum of an explicit Kelvin tensor and a complementary part in terms of a line integral over $[0, \pi]$. It is emphasized that in (4.1) and (4.2), the eigenvalues $p_J$, the eigenmatrix $\boldsymbol{A}$, and the matrix $\boldsymbol{K}$ are functions of $\theta$, with $p_J$ ($J = 1, 2, 3, 4$) and $\boldsymbol{A} = [\boldsymbol{a}_1, \boldsymbol{a}_2, \boldsymbol{a}_3, \boldsymbol{a}_4]$ being the eigensolutions of (3.3) for a given $\theta$. We further remark that under the assumption of 2D deformation, the corresponding displacement tensor can be derived analytically (without any line integral), as given in Appendix A.

Similarly, the half-space traction and in-plane stress tensors can be obtained as

$$\left.\begin{aligned} \boldsymbol{T}(\boldsymbol{x}; \boldsymbol{d}) &= \boldsymbol{T}^{\infty}(\boldsymbol{x}; \boldsymbol{d}) + \frac{1}{2\pi^2} \int_0^{\pi} \bar{\boldsymbol{B}} \boldsymbol{G}_2 \boldsymbol{A}^{\mathrm{T}} \, \mathrm{d}\theta, \\ \boldsymbol{S}(\boldsymbol{x}; \boldsymbol{d}) &= \boldsymbol{S}^{\infty}(\boldsymbol{x}; \boldsymbol{d}) + \frac{1}{2\pi^2} \int_0^{\pi} \bar{\boldsymbol{C}} \boldsymbol{G}_2 \boldsymbol{A}^{\mathrm{T}} \, \mathrm{d}\theta. \end{aligned}\right\} \tag{4.3}$$

Again, in (4.3), $\boldsymbol{T}^{\infty}(\boldsymbol{x}; \boldsymbol{d})$ and $\boldsymbol{S}^{\infty}(\boldsymbol{x}; \boldsymbol{d})$ denote the Green's traction and in-plane stress tensors in an anisotropic and piezoelectric full-space (Pan & Tonon 2000), and

$$(\boldsymbol{G}_2)_{IJ} = \frac{(\bar{\boldsymbol{K}}^{-1}\boldsymbol{K})_{IJ}}{\{-\bar{p}_I z + p_J d - [(x_1 - d_1)\cos\theta + (x_2 - d_2)\sin\theta]\}^2}. \tag{4.4}$$

† Thereafter, the indices $I$ and $J$ take the range from 1 to 4.

In analysis of certain problems based upon the integral equation method, the derivatives of the Green's displacements and stresses with respect to the source point $(d_1, d_2, d_3)$ are also required (Pan 1999). They are found to be (for $j = 1, 2, 3$)

$$\frac{\partial \boldsymbol{U}(\boldsymbol{x};\boldsymbol{d})}{\partial d_j} = \frac{\partial \boldsymbol{U}^{\infty}(\boldsymbol{x};\boldsymbol{d})}{\partial d_j} - \frac{1}{2\pi^2}\int_0^{\pi} \bar{A}\boldsymbol{G}_2\langle g_j\rangle \boldsymbol{A}^{\mathrm{T}}\,\mathrm{d}\theta, \tag{4.5}$$

$$\left.\begin{aligned} \langle g_1\rangle &= \mathrm{diag}[\cos\theta, \cos\theta, \cos\theta, \cos\theta],\\ \langle g_2\rangle &= \mathrm{diag}[\sin\theta, \sin\theta, \sin\theta, \sin\theta],\\ \langle g_3\rangle &= \mathrm{diag}[p_1, p_2, p_3, p_4], \end{aligned}\right\} \tag{4.6}$$

$$\left.\begin{aligned} \frac{\partial \boldsymbol{T}(\boldsymbol{x};\boldsymbol{d})}{\partial d_j} &= \frac{\partial \boldsymbol{T}^{\infty}(\boldsymbol{x};\boldsymbol{d})}{\partial d_j} - \frac{1}{2\pi^2}\int_0^{\pi} \bar{\boldsymbol{B}}\boldsymbol{G}_3\langle g_j\rangle \boldsymbol{A}^{\mathrm{T}}\,\mathrm{d}\theta,\\ \frac{\partial \boldsymbol{S}(\boldsymbol{x};\boldsymbol{d})}{\partial d_j} &= \frac{\partial \boldsymbol{S}^{\infty}(\boldsymbol{x};\boldsymbol{d})}{\partial d_j} - \frac{1}{2\pi^2}\int_0^{\pi} \bar{\boldsymbol{C}}\boldsymbol{G}_3\langle g_j\rangle \boldsymbol{A}^{\mathrm{T}}\,\mathrm{d}\theta, \end{aligned}\right\} \tag{4.7}$$

$$(\boldsymbol{G}_3)_{IJ} = \frac{(\bar{\boldsymbol{K}}^{-1}\boldsymbol{K})_{IJ}}{\{-\bar{p}_I z + p_J d - [(x_1 - d_1)\cos\theta + (x_2 - d_2)\sin\theta]\}^3}. \tag{4.8}$$

Equations (4.1), (4.3), (4.5) and (4.7) are the generalized Mindlin solutions, or the *complete* Green's functions under general boundary conditions in an anisotropic and piezoelectric half-space. It is emphasized that these generalized Mindlin solutions are presented in a unified form so that the 16 different sets of boundary conditions (2.11) are all included. To find the Mindlin solution for a given set of boundary conditions, one only needs to assign the corresponding $\boldsymbol{K}$ matrix. With the exception of the solution to the traction-free insulating boundary condition (Pan & Yuan 2000), solutions to all other boundary conditions are presented for the first time in this paper. Since the solutions include all the 16 different sets of boundary conditions, it is particularly convenient in investigating the effect of different boundary conditions on the elastic and electric fields based on the present Mindlin solutions.

Considering the complicated nature of the problem and simplicity of the final expression of the Mindlin solution, it is seen that by resorting to the superposition method, the extended Stroh formalism is indeed a very powerful and elegant method. A direct Fourier transform method would require a 3D Fourier integral for the full-space Green's functions and 4D Fourier integral for the complementary part (Walker 1993). Furthermore, under the assumption of 2D deformation, the corresponding half-plane solutions can be derived analytically by following a similar procedure, as shown in Appendix A.

It is also noticed that when the source point is within the half-space (i.e. $d \neq 0$), the integrals in (4.1), (4.3), (4.5) and (4.7) are regular and thus can be easily carried out by a standard numerical integral method such as the Gauss quadrature. When the source point is on the surface, the generalized Mindlin solution is then reduced to the generalized Boussinesq solution (i.e. $z \neq 0$, $d = 0$); when the field and source points are both on the surface (i.e. $z = d = 0$), the solution is further reduced to the so-called surface Green's function. A detailed study on these special cases of the generalized Mindlin solution was given in Pan (2002*b*) for the purely elastic case.

## 5. Effects of surface boundary conditions

Besides the elastic and electric coupling in an anisotropic piezoelectric half-space, another important issue is the effect of different surface conditions on the elastic and electric fields. Ru (2001) first studied the 2D piezoelectric Eshelby's problem of an arbitrarily shaped inclusion. For either traction-free or rigid mechanical condition combined with either an insulating or conducting condition on the surface, he derived analytically the elastic and electric quantities due to an inclusion of arbitrary shape, and discussed the corrections to these quantities if an insulating, instead of a conducting, surface was assumed, or vice versa (Ru 2001).

Stimulated by Ru's analysis (2001), we now study the effects of surface boundary conditions on the elastic and electric fields in a 3D anisotropic and piezoelectric half-space. In contrast to the work of Ru (2001), our physical model is 3D with a concentrated point source, namely, a generalized Mindlin's problem. Furthermore, the present study covers 16 different sets of surface boundary conditions.

When studying the correction to, or difference of, the elastic and electric quantities due to different surface boundary conditions, we remark on an interesting feature. The generalized Kelvin solution (i.e. the infinite Green's function) has no influence at all to the correction. It is the complementary part of the generalized Mindlin solution that contributes the correction! We also notice that it is the compound matrix $\bar{\boldsymbol{K}}^{-1}\boldsymbol{K}$ that totally controls such a correction. This is actually not surprising since when deriving the Mindlin solution, it is the complementary part that takes care of the different surface boundary conditions, and it is the compound matrix $\bar{\boldsymbol{K}}^{-1}\boldsymbol{K}$ that directly accomplishes the task! Therefore, the correction to the elastic and electric quantities is directly proportional to the difference of the integral of the compound matrix $\bar{\boldsymbol{K}}^{-1}\boldsymbol{K}$.

In the study presented below, we restrict ourselves to the four common surface conditions, namely, the traction-free insulating and conducting, and rigid insulating and conducting conditions. Other surface conditions, such as the slippery insulating and conducting surfaces, can be investigated following a similar procedure. Furthermore, our expressions for the extended displacement and stress fields are for the source point $\boldsymbol{d}$ within the half-space ($d \neq 0$) and the field point $\boldsymbol{x}$ anywhere in the half-space. The surface response is a particular case where the field point is on the surface of the half-space (i.e. $z = 0$). We also mention that results for the derivatives of the extended displacements and stresses will not be given but can be obtained similarly.

### (a) *Effects of surface mechanical conditions*

To find the effect of different surface mechanical conditions on the field quantities, we assume that the electric surface condition is either insulating or conducting. For an insulating surface, the correction to the extended displacement tensor is found as

$$\boldsymbol{U}(\boldsymbol{x};\boldsymbol{d})_{\mathrm{fi}} - \boldsymbol{U}(\boldsymbol{x};\boldsymbol{d})_{\mathrm{ri}} = \frac{1}{2\pi^2}\int_0^{\pi} \bar{A}\boldsymbol{G}_{1\mathrm{fr}}\boldsymbol{A}^{\mathrm{T}}\,\mathrm{d}\theta, \tag{5.1}$$

where

$$(\boldsymbol{G}_{1\mathrm{fr}})_{IJ} = \frac{[(\bar{\boldsymbol{K}}_{\mathrm{fi}}^{-1}\boldsymbol{K}_{\mathrm{fi}}) - (\bar{\boldsymbol{K}}_{\mathrm{ri}}^{-1}\boldsymbol{K}_{\mathrm{ri}})]_{IJ}}{-\bar{p}_I z + p_J d - [(x_1 - d_1)\cos\theta + (x_2 - d_2)\sin\theta]}. \tag{5.2}$$

The first subscript 'f' ('r') to $\boldsymbol{U}$ and $\bar{\boldsymbol{K}}^{-1}\boldsymbol{K}$ denotes traction-free (rigid) boundary conditions, and the second subscript 'i' to them denotes the insulating surface.

Similarly, the correction to the extended traction and in-plane stress tensors are

$$\boldsymbol{T}(\boldsymbol{x};\boldsymbol{d})_{\mathrm{fi}} - \boldsymbol{T}(\boldsymbol{x};\boldsymbol{d})_{\mathrm{ri}} = \frac{1}{2\pi^2}\int_0^{\pi} \bar{\boldsymbol{B}}\boldsymbol{G}_{2\mathrm{fr}}\boldsymbol{A}^{\mathrm{T}}\,\mathrm{d}\theta, \tag{5.3}$$

$$\boldsymbol{S}(\boldsymbol{x};\boldsymbol{d})_{\mathrm{fi}} - \boldsymbol{S}(\boldsymbol{x};\boldsymbol{d})_{\mathrm{ri}} = \frac{1}{2\pi^2}\int_0^{\pi} \bar{\boldsymbol{C}}\boldsymbol{G}_{2\mathrm{fr}}\boldsymbol{A}^{\mathrm{T}}\,\mathrm{d}\theta, \tag{5.4}$$

where

$$(\boldsymbol{G}_{2\mathrm{fr}})_{IJ} = \frac{[(\bar{\boldsymbol{K}}_{\mathrm{fi}}^{-1}\boldsymbol{K}_{\mathrm{fi}}) - (\bar{\boldsymbol{K}}_{\mathrm{ri}}^{-1}\boldsymbol{K}_{\mathrm{ri}})]_{IJ}}{\{-\bar{p}_I z + p_J d - [(x_1 - d_1)\cos\theta + (x_2 - d_2)\sin\theta]\}^2}. \tag{5.5}$$

Equations (5.1), (5.3) and (5.4) clearly show that the effect of different mechanical boundary conditions on the extended displacement and stress fields is controlled by the difference of the compound matrix $\bar{\boldsymbol{K}}^{-1}\boldsymbol{K}$ under the traction-free insulating ('fi') and rigid insulating ('ri') boundary conditions.

To obtain the effect of different mechanical boundary conditions on the extended displacement and stress fields for a given conducting surface, one can simply replace the difference of the compound matrix $\bar{\boldsymbol{K}}^{-1}\boldsymbol{K}$ under the 'fi' and 'ri' boundary conditions with the difference of the compound matrix $\bar{\boldsymbol{K}}^{-1}\boldsymbol{K}$ under the 'fc' and 'rc' boundary conditions. Formally, this is to replace the subscript 'i' with the subscript 'c'.

### (*b*) *Effects of surface electric conditions*

Similarly, to see the effect of different surface electric conditions on the field quantities for a traction-free or rigid surface, we only need to find the difference of the integral of the compound matrix $\bar{\boldsymbol{K}}^{-1}\boldsymbol{K}$. For traction-free surface, the correction to the extended displacement tensor is found to be

$$\boldsymbol{U}(\boldsymbol{x};\boldsymbol{d})_{\mathrm{fi}} - \boldsymbol{U}(\boldsymbol{x};\boldsymbol{d})_{\mathrm{fc}} = \frac{1}{2\pi^2}\int_0^{\pi} \bar{A}\boldsymbol{G}_{1\mathrm{ic}}\boldsymbol{A}^{\mathrm{T}}\,\mathrm{d}\theta, \tag{5.6}$$

where

$$(\boldsymbol{G}_{1\mathrm{ic}})_{IJ} = \frac{[(\bar{\boldsymbol{K}}_{\mathrm{fi}}^{-1}\boldsymbol{K}_{\mathrm{fi}}) - (\bar{\boldsymbol{K}}_{\mathrm{fc}}^{-1}\boldsymbol{K}_{\mathrm{fc}})]_{IJ}}{-\bar{p}_I z + p_J d - [(x_1 - d_1)\cos\theta + (x_2 - d_2)\sin\theta]}. \tag{5.7}$$

The correction to the corresponding extended traction and in-plane stress tensors are found to be

$$\boldsymbol{T}(\boldsymbol{x};\boldsymbol{d})_{\mathrm{fi}} - \boldsymbol{T}(\boldsymbol{x};\boldsymbol{d})_{\mathrm{fc}} = \frac{1}{2\pi^2}\int_0^{\pi} \bar{\boldsymbol{B}}\boldsymbol{G}_{2\mathrm{ic}}\boldsymbol{A}^{\mathrm{T}}\,\mathrm{d}\theta, \tag{5.8}$$

$$\boldsymbol{S}(\boldsymbol{x};\boldsymbol{d})_{\mathrm{fi}} - \boldsymbol{S}(\boldsymbol{x};\boldsymbol{d})_{\mathrm{fc}} = \frac{1}{2\pi^2}\int_0^{\pi} \bar{\boldsymbol{C}}\boldsymbol{G}_{2\mathrm{ic}}\boldsymbol{A}^{\mathrm{T}}\,\mathrm{d}\theta, \tag{5.9}$$

where

$$(\boldsymbol{G}_{2\mathrm{ic}})_{IJ} = \frac{[(\bar{\boldsymbol{K}}_{\mathrm{fi}}^{-1}\boldsymbol{K}_{\mathrm{fi}}) - (\bar{\boldsymbol{K}}_{\mathrm{fc}}^{-1}\boldsymbol{K}_{\mathrm{fc}})]_{IJ}}{\{-\bar{p}_I z + p_J d - [(x_1 - d_1)\cos\theta + (x_2 - d_2)\sin\theta]\}^2}. \tag{5.10}$$

Again, if we replace the traction-free boundary condition by the rigid boundary condition, then the effect of different electric surface conditions on the elastic and

electric quantities for a mechanically rigid surface can be obtained. This is done by simply replacing the difference of the compound matrix $\bar{\boldsymbol{K}}^{-1}\boldsymbol{K}$ under the 'fi' and 'fc' boundary conditions with the difference of the compound matrix $\bar{\boldsymbol{K}}^{-1}\boldsymbol{K}$ under the 'ri' and 'rc' boundary conditions.

## 6. Numerical examples

Having derived the generalized Mindlin solution and discussed the effect of different boundary conditions on the elastic and electric quantities, we now present numerical examples on the variation of these quantities on the surface when a point source is applied within the half-space. Two typical piezoelectric materials are selected for the half-space. One is a left-hand quartz in a rotated coordinate system (Tiersten 1969) with elastic constants, piezoelectric coefficients, and dielectric constants being, respectively,

$$[C] = \begin{bmatrix} 0.8674 & -0.0825 & 0.2715 & -0.0366 & 0 & 0 \\ -0.0825 & 1.2977 & -0.0742 & 0.057 & 0 & 0 \\ 0.2715 & -0.0742 & 1.0283 & 0.0992 & 0 & 0 \\ -0.0366 & 0.057 & 0.0992 & 0.3861 & 0 & 0 \\ 0 & 0 & 0 & 0 & 0.6881 & 0.0253 \\ 0 & 0 & 0 & 0 & 0.0253 & 0.2901 \end{bmatrix} \quad (10^{11}\ \mathrm{N\ m^{-2}}), \tag{6.1}$$

$$[e] = \begin{bmatrix} 0.171 & -0.152 & -0.0187 & 0.067 & 0 & 0 \\ 0 & 0 & 0 & 0 & 0.108 & -0.095 \\ 0 & 0 & 0 & 0 & -0.0761 & 0.067 \end{bmatrix} \quad (\mathrm{C\ m^{-2}}), \tag{6.2}$$

$$[\varepsilon] = \begin{bmatrix} 0.3921 & 0 & 0 \\ 0 & 0.3982 & 0.0086 \\ 0 & 0.0086 & 0.4042 \end{bmatrix} \quad (10^{-10}\ \mathrm{C\ V^{-1}\ m^{-1}}). \tag{6.3}$$

Another one is the poled lead–zirconate–titanate (PZT-4) ceramic (Dunn & Taya 1993) with elastic constants, piezoelectric coefficients, and dielectric constants being, respectively,

$$[C] = \begin{bmatrix} 1.39 & 0.778 & 0.743 & 0 & 0 & 0 \\ 0.778 & 1.39 & 0.743 & 0 & 0 & 0 \\ 0.743 & 0.743 & 1.15 & 0 & 0 & 0 \\ 0 & 0 & 0 & 0.256 & 0 & 0 \\ 0 & 0 & 0 & 0 & 0.256 & 0 \\ 0 & 0 & 0 & 0 & 0 & 0.306 \end{bmatrix} \quad (10^{11}\ \mathrm{N\ m^{-2}}), \tag{6.4}$$

$$[e] = \begin{bmatrix} 0 & 0 & 0 & 0 & 12.7 & 0 \\ 0 & 0 & 0 & 12.7 & 0 & 0 \\ -5.2 & -5.2 & 15.1 & 0 & 0 & 0 \end{bmatrix} \quad (\mathrm{C\ m^{-2}}), \tag{6.5}$$

$$[\varepsilon] = \begin{bmatrix} 0.646\,05 & 0 & 0 \\ 0 & 0.646\,05 & 0 \\ 0 & 0 & 0.561\,975 \end{bmatrix} \quad (10^{-8}\ \mathrm{C\ V^{-1}\ m^{-1}}). \tag{6.6}$$

It is seen that the quartz belongs to the monoclinic system in class 2 with $x$ being the diagonal axis, while the ceramic belongs to the hexagonal system in class 6 mm with $z$

in the poling direction (Tiersten 1969). Furthermore, the quartz is a weakly coupled piezoelectric material and the ceramic is a strongly coupled one. Actually, using the dimensionless parameter, $g$, which indicates the degree of the electromechanical coupling (Adachi 1985; Suo *et al.* 1992), defined as $g = e_{\max}/\sqrt{(\varepsilon_{\max} C_{\max})}$, we found that $g$ equals 0.07 and 0.5, respectively, for the quartz and ceramic. We remark that for semiconductors GaAs and AlN, the parameter $g$ is roughly 0.04 and 0.25, respectively (Adachi 1985; Chin *et al.* 1994; Mohammad & Morkoc 1996; Bernardini *et al.* 1997; Wright 1997). Thus, while GaAs is a weakly coupled material, AlN is a strongly coupled one.

Numerical results are presented for the dimensionless stress and electric displacement, caused by a point force or a negative point electric charge (see (2.1) and (2.10)). While the source is fixed at $\boldsymbol{d} = (0, 0, 1)$, the field point varies on the surface of the half-space as $\boldsymbol{z} = (x, x, 0)$, $x \in [-1, 1]$, with the dimensional coordinate being recovered by simply multiplying $L$ (= 1 m). Also, in order to obtain the dimensional stress and electric displacement (i.e. for stress in N m$^{-2}$ and electric displacement in C m$^{-2}$), one needs only to carry out the following simple multiplication or division (with $C_{\max} = 1.2977 \times 10^{11}$ N m$^{-2}$ and $E_{\max} = 0.171$ C m$^{-2}$ for the quartz, and $C_{\max} = 1.39 \times 10^{11}$ N m$^{-2}$ and $E_{\max} = 15.1$ C m$^{-2}$ for the ceramic):

(i) for the stress due to a point force (F1 and F3 in the figures), divide the results by $L^2$;

(ii) for the stress due to a negative electric charge (F4 in the figures), multiply the results by $C_{\max}/(E_{\max} L^2)$;

(iii) for the electric displacement due to a point force, multiply the results by $E_{\max}/(C_{\max} L^2)$;

(iv) for the electric displacement due to a negative electric charge, divide the results by $L^2$.

In each figure, four curves are plotted: a solid line with solid triangles for the traction-free insulating surface (ins, traction-free); a dashed line with open triangles for the traction-free conducting surface (con, traction-free); a solid line with solid diamonds for the rigid insulating surface (ins, rigid); and a dashed line with open diamonds for the rigid conducting surface (con, rigid). In so doing, the corrections to the field quantities due to different surface conditions, discussed in the previous section, can be observed directly from these figures. Furthermore, according to the field and source types, the results are grouped into four cases and are discussed below.

### (*a*) *Electric response due to a mechanical point source*

Parts (*a*) and (*b*) of figure 1 show, respectively, the variation of the normalized electric displacements $D_x$ and $D_z$ on the surface of the quartz half-space due to a point force in the $z$-direction (i.e. F3). The corresponding $D_x$ and $D_z$ on the surface of the ceramic half-space are plotted in figure 1*c*, *d*. (They are either symmetric or anti-symmetric about $x = 0$ since the ceramic is hexagonal or transversely isotropic.) It is observed from these figures that different surface boundary conditions can cause significant difference on the electric response when a mechanical point source is

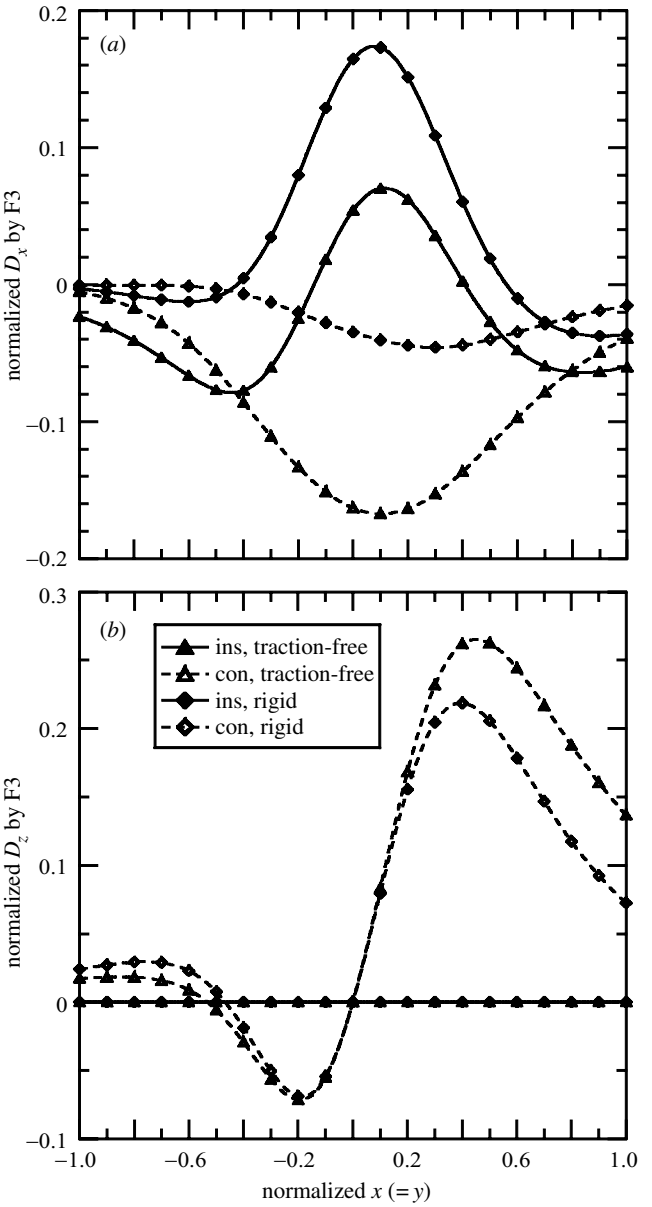


Figure 1. Variations of the normalized electric displacements $D_x$ and $D_z$ on the surface ($z = 0$) of the quartz ($a$) and ($b$) half-spaces due to a point force applied at $\boldsymbol{d} = (0, 0, 1)$ in the $z$-direction, for the traction-free insulating (ins, traction-free), traction-free conducting (con, traction-free), rigid insulating (ins, rigid), and rigid conducting (con, rigid) surface conditions.

applied (similar features have been also observed by the author when a point force is applied in the $x$-direction). Therefore, in general, a coupled piezoelectric model should be used. Otherwise, the electric components $D_x$ and $D_z$ would be zero if an uncoupled model is used, which is obviously contradictory to what we have observed in figure $1a, b$ for the fully coupled model.

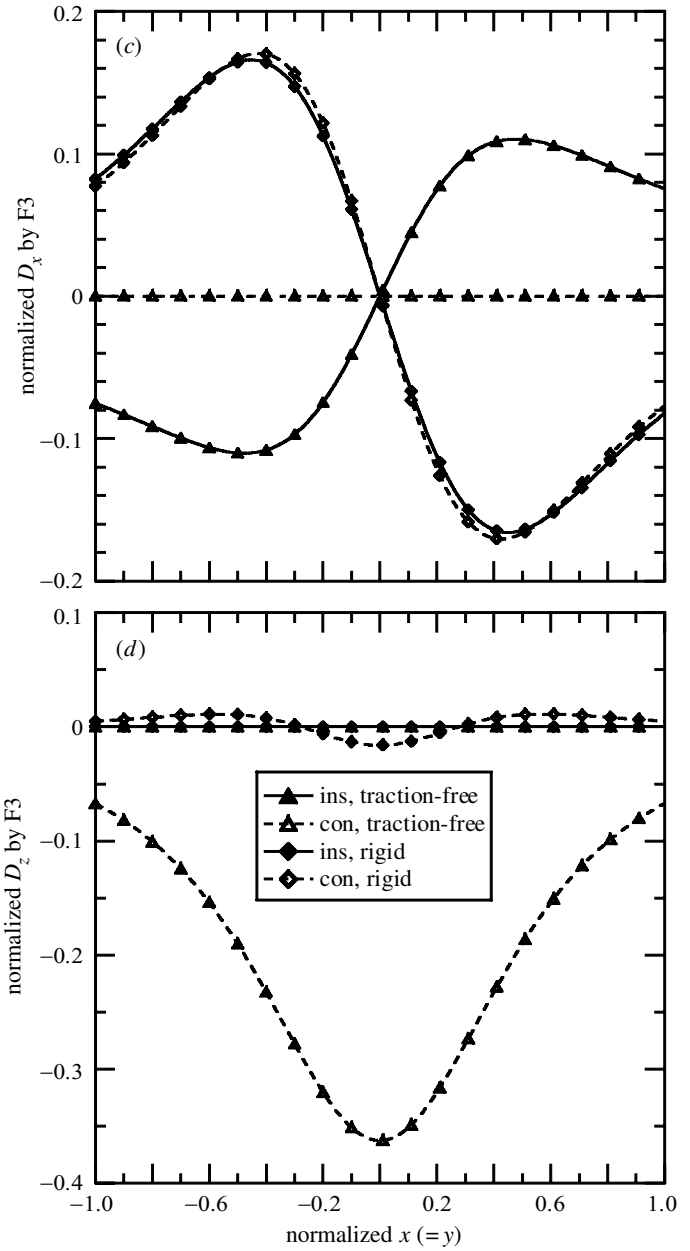


Figure 1. (*Cont.*) Variations of the normalized electric displacements $D_x$ and $D_z$ on the surface ($z = 0$) of the ceramic (*c*) and (*d*) half-spaces due to a point force applied at $\boldsymbol{d} = (0, 0, 1)$ in the $z$-direction, for the traction-free insulating (ins, traction-free), traction-free conducting (con, traction-free), rigid insulating (ins, rigid), and rigid conducting (con, rigid) surface conditions.

### (*b*) *Mechanical response due to an electric point source*

While parts (*a*) and (*b*) of figure 2 show, respectively, the variation of the normalized stress components $\sigma_{xx}$ and $\sigma_{zz}$ on the surface of the quartz half-space due to a

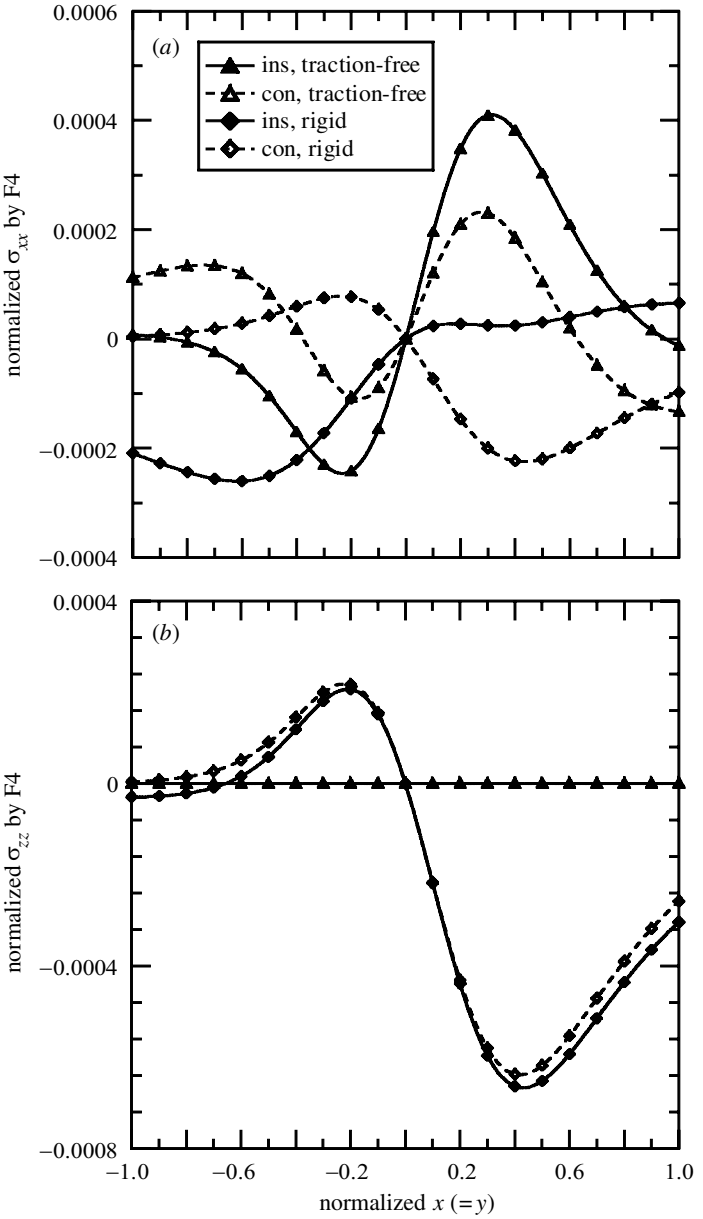


Figure 2. Variations of the normalized stress components $\sigma_{xx}$ and $\sigma_{zz}$ on the surface ($z = 0$) of the quartz ($a$) and ($b$) half-spaces due to a negative point electric charge applied at $\boldsymbol{d} = (0, 0, 1)$, for the traction-free insulating (ins, traction-free), traction-free conducting (con, traction-free), rigid insulating (ins, rigid), and rigid conducting (con, rigid) surface conditions.

negative point electric charge (i.e. F4), parts ($c$) and ($d$) of figure 2 show the corresponding variation of $\sigma_{xx}$ and $\sigma_{zz}$ on the surface of the ceramic half-space. It is seen that, except for $\sigma_{zz}$ in the vicinity of the epicentre of the quartz half-space, different boundary conditions predict completely different surface stresses if a point electric

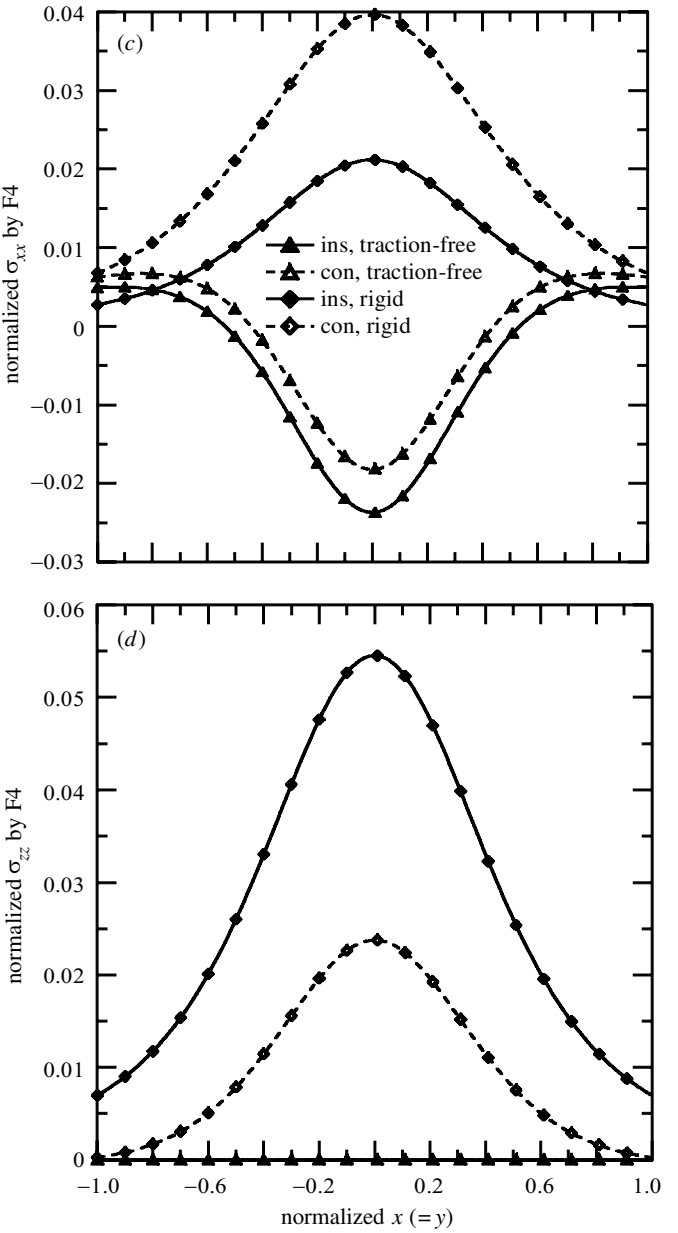


Figure 2. (*Cont.*) Variations of the normalized stress components $\sigma_{xx}$ and $\sigma_{zz}$ on the surface ($z = 0$) of the ceramic ($c$) and ($d$) half-spaces due to a negative point electric charge applied at $\boldsymbol{d} = (0, 0, 1)$, for the traction-free insulating (ins, traction-free), traction-free conducting (con, traction-free), rigid insulating (ins, rigid), and rigid conducting (con, rigid) surface conditions.

charge is applied within the half-space. Again, for this case, the coupled piezoelectric model needs to be used, even for the weakly coupled quartz half-space. An uncoupled purely electric model would have no influence on the mechanical response of the uncoupled system.

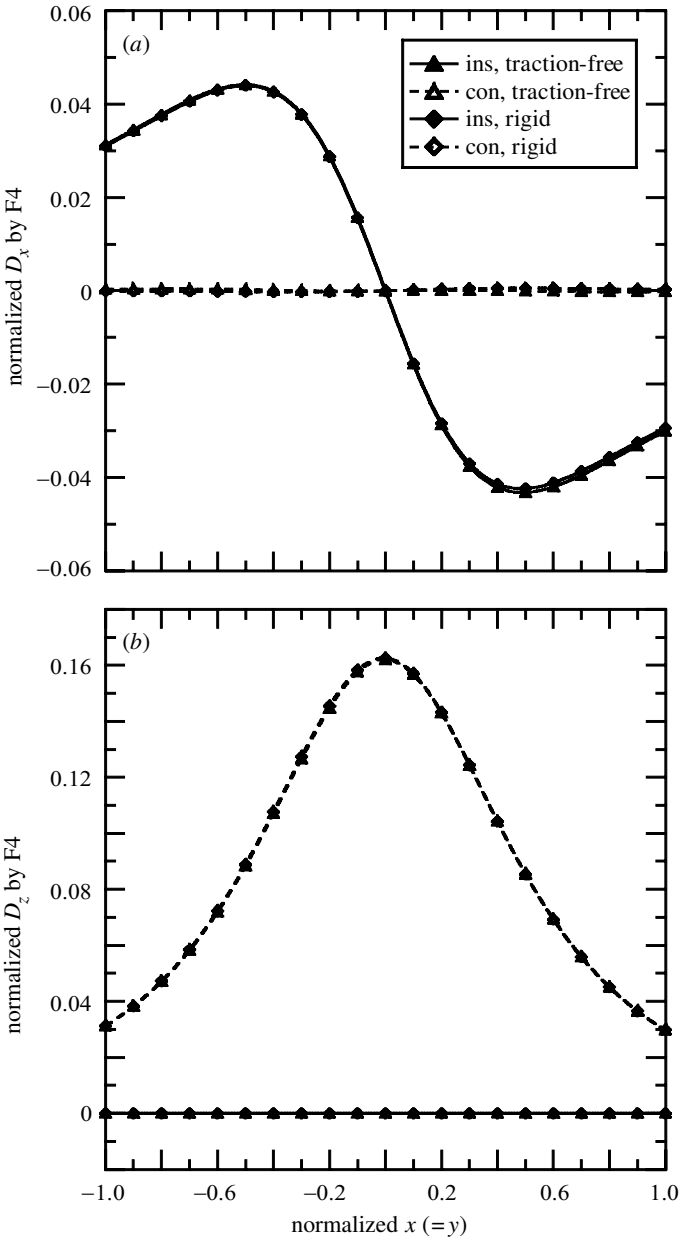


Figure 3. Variations of the normalized electric displacement components $D_x$ and $D_z$ on the surface ($z = 0$) of the quartz ($a$) and ($b$) half-spaces due to a negative point electric charge applied at $\boldsymbol{d} = (0, 0, 1)$, for the traction-free insulating (ins, traction-free), traction-free conducting (con, traction-free), rigid insulating (ins, rigid), and rigid conducting (con, rigid) surface conditions.

### ($c$) *Electric response due to an electric point source*

Parts ($a$) and ($b$) of figure 3 show the variation of the normalized electric displacement components $D_x$ and $D_z$, respectively, on the surface of the quartz half-space

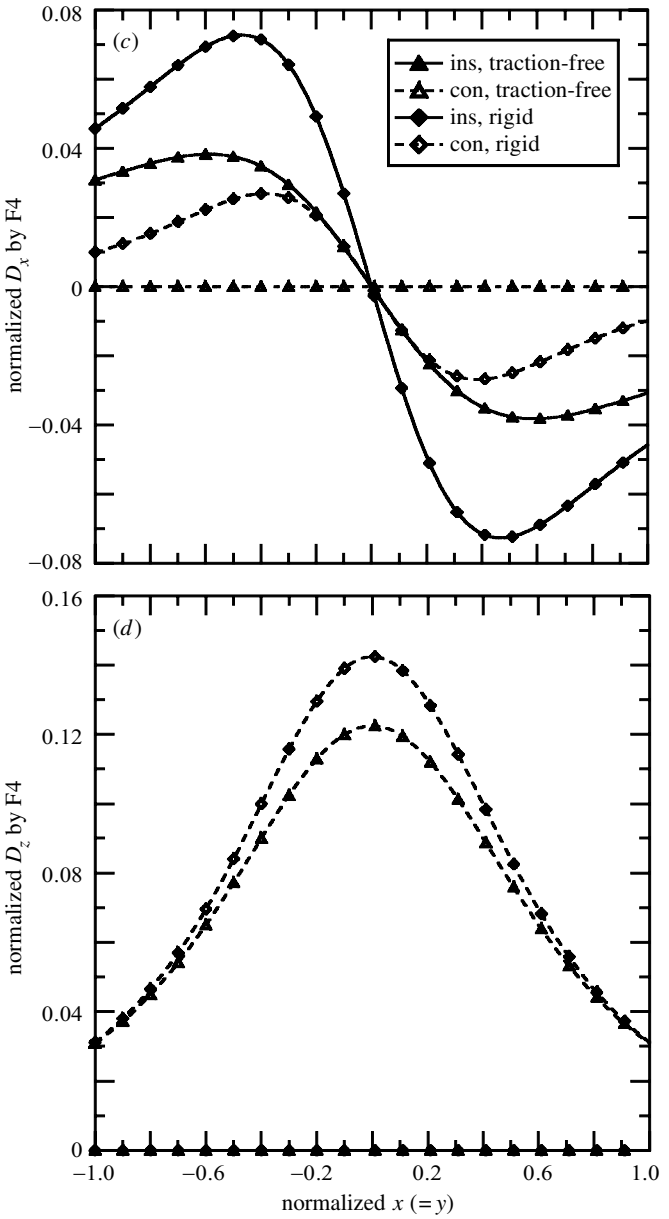


Figure 3. (*Cont.*) Variations of the normalized electric displacement components $D_x$ and $D_z$ on the surface ($z = 0$) of the ceramic ($c$) and ($d$) half-spaces due to a negative point electric charge applied at $\boldsymbol{d} = (0, 0, 1)$, for the traction-free insulating (ins, traction-free), traction-free conducting (con, traction-free), rigid insulating (ins, rigid), and rigid conducting (con, rigid) surface conditions.

due to a negative point electric charge. The corresponding $D_x$ and $D_z$ on the surface of the ceramic half-space are plotted in figure $3c, d$. For the quartz half-space (figure $3a, b$), it is observed that the two curves corresponding to the traction-free and rigid conditions are nearly identical to each other for the given electric boundary

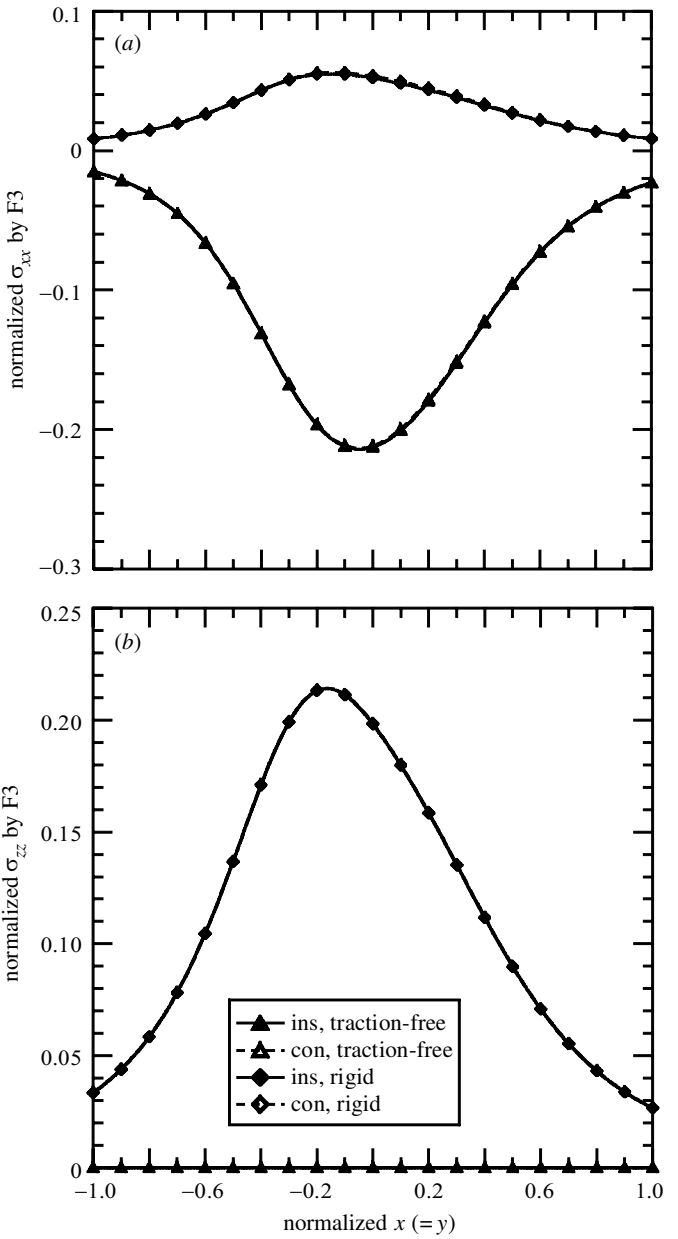


Figure 4. Variations of the normalized stress components $\sigma_{xx}$ and $\sigma_{zz}$ on the surface ($z = 0$) of the quartz ($a$) and ($b$) half-spaces due to a point force applied at $\boldsymbol{d} = (0, 0, 1)$ in the $z$-direction, for the traction-free insulating (ins, traction-free), traction-free conducting (con, traction-free), rigid insulating (ins, rigid), and rigid conducting (con, rigid) surface conditions.

condition (insulating or conducting). Therefore, the electric response on the surface of the quartz half-space (i.e. with weak coupling) is mainly controlled by the electric boundary condition and can be analysed using the corresponding uncoupled purely electric model. However, for the strongly coupled ceramic half-space, the fully

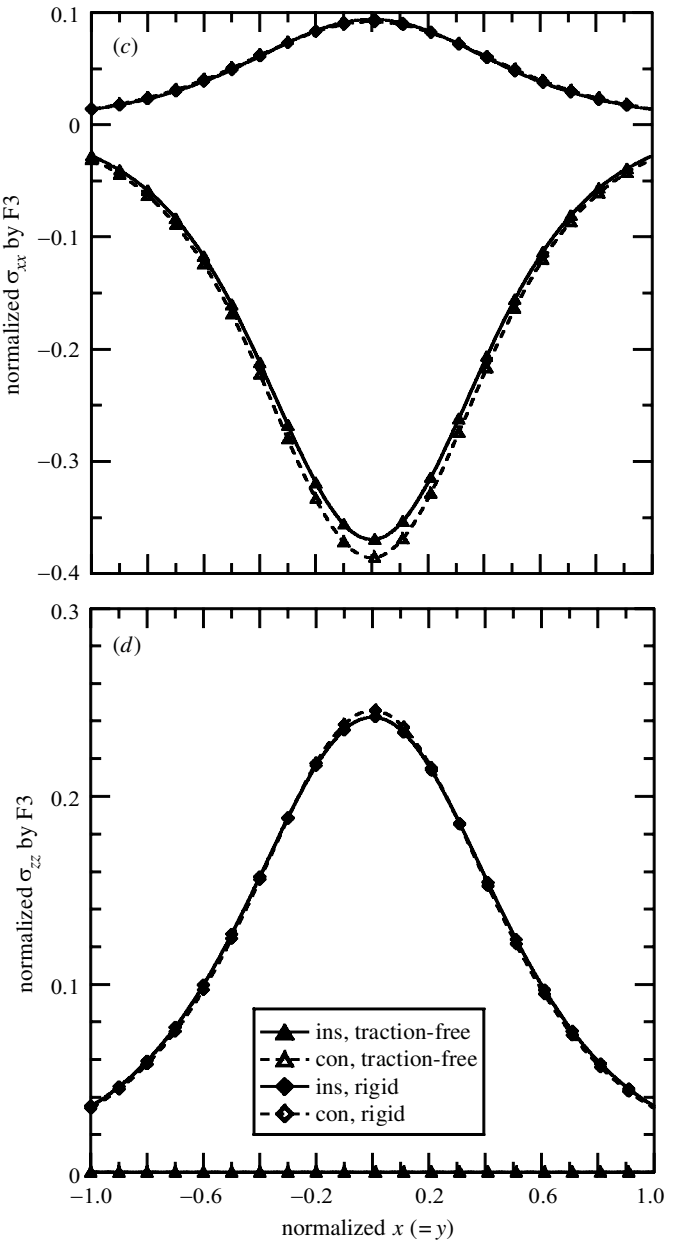


Figure 4. (*Cont.*) Variations of the normalized stress components $\sigma_{xx}$ and $\sigma_{zz}$ on the surface ($z = 0$) of the ceramic ($c$) and ($d$) half-spaces due to a point force applied at $\boldsymbol{d} = (0, 0, 1)$ in the $z$-direction, for the traction-free insulating (ins, traction-free), traction-free conducting (con, traction-free), rigid insulating (ins, rigid), and rigid conducting (con, rigid) surface conditions.

coupled piezoelectric model must be used, as is clearly shown in figure 3$c, d$, where different mechanical surface conditions predict substantially different $D_x$ and $D_z$. It is particularly interesting that while an uncoupled purely electric model causes the horizontal electric displacement ($D_x$ and $D_y$) to be zero on the conducting sur-

face, the corresponding fully coupled model predicts a non-zero horizontal electric displacement on the surface under the rigid conducting condition (figure 3*c*).

### (*d*) *Mechanical response due to a mechanical point source*

While the normalized stress components $\sigma_{xx}$ and $\sigma_{zz}$ on the surface of the quartz half-space due to a point force in the $z$-direction are plotted, respectively, in parts (*a*) and (*b*) of figure 4, the corresponding $\sigma_{xx}$ and $\sigma_{zz}$ on the surface of the ceramic half-space are depicted in figure 4*c*, *d*. It is apparent that, for the quartz half-space, the surface stresses are mainly controlled by the mechanical boundary conditions, and therefore the corresponding uncoupled purely elastic model can be adopted to simplify the analysis (figure 4*a*, *b*). However, for the strongly coupled ceramic half-space (figure 4*c*, *d*), the corresponding uncoupled elastic model is found to be suitable only in the vicinity of $x = 0$ on the surface with a relatively large error tolerance (say *ca.* 10%). We finally remark that a similar feature has also been observed for the stress components due to a point force in the $x$-direction.

## 7. Conclusions

In this paper, we have solved Mindlin's problem in an anisotropic and piezoelectric half-space with 16 different sets of surface boundary conditions. The generalized Mindlin solution is derived based on the extended Stroh formalism and 2D Fourier transforms in combination with Mindlin's superposition method, and is expressed as a sum of the generalized Kelvin solution and a complementary part. While the former is in an explicit form, as previously derived by Pan & Tonon (2000), the latter is expressed in terms of a simple line integral over $[0, \pi]$. Of the 16 different sets, only the solution to the traction-free insulating surface was solved before (Pan & Yuan 2000); solutions to other 15 sets of boundary conditions are presented for the first time. Furthermore, by following a similar procedure, we have also derived analytically the corresponding 2D solutions for the 16 different sets of surface boundary conditions.

The effect of different surface conditions on the elastic and electric quantities has been studied and discussed in detail for the four common surface conditions, namely, traction-free insulating and conducting, and rigid insulating and conducting conditions. To illustrate the significance of different boundary conditions as well as the electromechanical coupling in piezoelectric problem analysis, numerical examples are carried out for two typical piezoelectric materials, namely, the quartz with weak coupling and ceramic with strong coupling. It is found that, if the point source is mechanical (electric), then the corresponding mechanical (electric) response on the surface of the half-space is nearly independent of the electric (mechanical) boundary conditions for the quartz. In other words, for these cases, the corresponding uncoupled purely elastic (electric) model could be employed to avoid the complexity due to the coupling. However, owning to its high degree of electromechanical coupling for the ceramic, the uncoupled purely elastic (electric) model is only applicable for certain quantities in the vicinity of $x = 0$ on the surface and should be adopted with caution. On the other hand, if one is also interested in the mechanical (electric) response on the surface of the half-space due to an electric (mechanical) point source, then the four different sets of boundary conditions can all significantly affect the surface response and the coupled (preferably the fully coupled) piezoelectric model must

be used, even if the electromechanical coupling is weak. These features are believed to be particularly useful in the study of the corresponding 3D Eshelby's problem and in the numerical modelling of strained quantum devices based on the Green's function method.

The author thanks Professor C. Q. Ru of the University of Alberta for valuable discussions and the two reviewers for their constructive comments.

## Appendix A. 2D piezoelectric half-plane Green's functions under general boundary conditions

Similar to the Mindlin's problem presented in the main text, we consider an anisotropic and piezoelectric half-space with its surface at $z = 0$. Here, however, we assume that the deformation is independent of the $y$-coordinate (i.e. the generalized plane strain deformation in the $(x, z)$ plane). We further let an extended line force $\boldsymbol{f} = (f_1, f_2, f_3, -q)$ and an extended line dislocation (i.e. a Burgers vector) $\boldsymbol{b} = (\Delta u_1, \Delta u_2, \Delta u_3, \Delta\phi)$ be applied at $(x, z) = (0, d)$ with $d > 0$. We remark that the half-plane Green's function for the traction-free insulating surface was derived previously using the one-complex-variable function approach (see, for example, Pan 1999). However, for the more general surface boundary conditions discussed in this paper, the Stroh formalism is found to be more convenient.

Similar to the purely elastic half-plane case (Ting 1996), it can be shown that the half-plane Green's functions (i.e. the extended displacement and stress function vectors) can be expressed as

$$\left.\begin{aligned} \boldsymbol{u} &= \frac{1}{\pi}\,\mathrm{Im}\{\boldsymbol{A}\langle\ln(z_* - p_* d)\rangle\boldsymbol{q}^{\infty}\} + \frac{1}{\pi}\,\mathrm{Im}\sum_{J=1}^{4}\{\boldsymbol{A}\langle\ln(z_* - \bar{p}_J d)\rangle\boldsymbol{q}_J\}, \\ \boldsymbol{\psi} &= \frac{1}{\pi}\,\mathrm{Im}\{\boldsymbol{B}\langle\ln(z_* - p_* d)\rangle\boldsymbol{q}^{\infty}\} + \frac{1}{\pi}\,\mathrm{Im}\sum_{J=1}^{4}\{\boldsymbol{B}\langle\ln(z_* - \bar{p}_J d)\rangle\boldsymbol{q}_J\}, \end{aligned}\right\} \tag{A 1}$$

where the extended stress function vector $\boldsymbol{\psi}$ is related to the elastic stresses and electrical displacements by

$$\sigma_{1J} = -\psi_{J,3}; \qquad \sigma_{3J} = \psi_{J,1}. \tag{A 2}$$

Also in (A 1), Im stands for the imaginary part, and $p_J$, $\boldsymbol{A}$, and $\boldsymbol{B}$ are the Stroh eigenvalues and eigenmatrices of the eigenequation (3.3) with the matrices $\boldsymbol{Q}$, $\boldsymbol{R}$, and $\boldsymbol{T}$ being defined by (3.4) in which $\theta = 0$. Finally, in (A 1),

$$\left.\begin{aligned} \langle\ln(z_* - p_* d)\rangle &= \mathrm{diag}[\ln(z_1 - p_1 d), \ln(z_2 - p_2 d), \ln(z_3 - p_3 d), \ln(z_4 - p_4 d)], \\ \langle\ln(z_* - \bar{p}_J d)\rangle &= \mathrm{diag}[\ln(z_1 - \bar{p}_J d), \ln(z_2 - \bar{p}_J d), \ln(z_3 - \bar{p}_J d), \ln(z_4 - \bar{p}_J d)], \end{aligned}\right\} \tag{A 3}$$

with the complex variable $z_J$ being defined by

$$z_J = x + p_J z. \tag{A 4}$$

It is noted that the first term in (A 1) corresponds to the full-plane Green's functions with

$$\boldsymbol{q}^{\infty} = \boldsymbol{A}^{\mathrm{T}}\boldsymbol{f} + \boldsymbol{B}^{\mathrm{T}}\boldsymbol{b}. \tag{A 5}$$

The second term in (A 1) is the complementary part of the solution with the complex constant vectors $\boldsymbol{q}_J$ $(J = 1, 2, 3, 4)$ to be determined. For the 16 sets of the surface boundary conditions discussed in § 2 of the main text, we define a new complex matrix $\boldsymbol{K}$ of $4 \times 4$ exactly the same way as for the 3D case (i.e. (3.18)), namely,

$$\boldsymbol{K} = \boldsymbol{I}_u \boldsymbol{A} + \boldsymbol{I}_t \boldsymbol{B}. \tag{A 6}$$

With this newly defined complex matrix $\boldsymbol{K}$, the involved complex constants in (A 1) can be found, in a remarkably simple and unified form, as

$$\boldsymbol{q}_J = \boldsymbol{K}^{-1} \bar{\boldsymbol{K}} \boldsymbol{I}_J \bar{\boldsymbol{q}}^{\infty}, \tag{A 7}$$

where the diagonal matrices $\boldsymbol{I}_J$ have the following diagonal elements:

$$\left.\begin{aligned} \boldsymbol{I}_1 &= \operatorname{diag}[1, 0, 0, 0]; \quad \boldsymbol{I}_2 = \operatorname{diag}[0, 1, 0, 0], \\ \boldsymbol{I}_3 &= \operatorname{diag}[0, 0, 1, 0]; \quad \boldsymbol{I}_4 = \operatorname{diag}[0, 0, 0, 1]. \end{aligned}\right\} \tag{A 8}$$

Thus, the extended displacement and stress function vectors in a generally anisotropic and piezoelectric half-plane with the 16 different sets of surface boundary conditions and due to an extended line force $\boldsymbol{f} = (f_1, f_2, f_3, -q)$ or an extended line dislocation $\boldsymbol{b} = (\Delta u_1, \Delta u_2, \Delta u_3, \Delta\phi)$ are all derived in a very concise form. Comparing the 2D solutions with the 3D ones, it is noted that while the eigenvalues, eigenmatrices, and the related matrices are constants (depend only upon the material properties) in the 2D solutions, their counterparts in 3D solutions are all functions of the Fourier transform variable $\theta$. Consequently, the 2D solutions are analytical while the 3D solutions involve a line integral for the variable $\theta$ over $[0, \pi]$.

With the extended displacement and stress function vectors being given by (A 1), their derivatives with respect to the field and source points can be analytically carried out and the resulting Green's functions can then be applied to various problems associated with a half-plane under general boundary conditions. It is remarked that, out of these 16 two-dimensional Green's solutions, only the solution to the traction-free insulating surface was solved before (see, for example, Pan 1999); solutions to other 15 sets of surface boundary conditions have not been reported in the literature.

## References


Adachi, S. 1985 GaAs, AlAs, and $Al_xGa_{1-x}As$: material parameters for use in research and device applications. *J. Appl. Phys.* **58**, R1–R29.

Akamatsu, M. & Tanuma, K. 1997 Green's function of anisotropic piezoelectricity. *Proc. R. Soc. Lond.* A **453**, 473–487.

Andreev, A. D., Downes, J. R., Faux, D. A. & O'Reilly, E. P. 1999 Strain distribution in quantum dots of arbitrary shape. *J. Appl. Phys.* **86**, 297–305.

Bacon, D. J., Barnett, D. M. & Scattergood, R. O. 1978 The anisotropic continuum theory of lattice defects. *Prog. Mater. Sci.* **23**, 51–262.

Barnett, D. M. & Lothe, J. 1975 Dislocations and line charges in anisotropic piezoelectric insulators. *Physica Status Solidi* B **67**, 105–111.

Bernardini, F., Fiorentini, V. & Vanderbilt, D. 1997 Spontaneous polarization and piezoelectric constants of III–V nitrides. *Phys. Rev.* B **56**, R10 024–R10 027.

Chen, W. Q. 1999 On the application of potential theory in piezoelasticity. *J. Appl. Mech.* **66**, 808–811.

Chen, W. Q., Shioya, T. & Ding, H. J. 1999 The elasto-electric field for a rigid conical punch on a transversely isotropic piezoelectric half-space. *J. Appl. Mech.* **66**, 764–771.

Chin, V. W. L., Tansley, T. L. & Osotchan, T. 1994 Electron mobilities in gallium, indium, and aluminum nitrides. *J. Appl. Phys.* **75**, 7365–7372.

Davies, J. H. 1998 Elastic and piezoelectric fields around a buried quantum dot: a simple picture. *J. Appl. Phys.* **84**, 1358–1365.

Davies, J. H. & Larkin, I. A. 1994 Theory of potential modulation in lateral surface superlattices. *Phys. Rev.* B **49**, 4800–4809.

Ding, H. J., Chen, B. & Liang, J. 1997 On the Green's functions for two-phase transversely isotropic piezoelectric media. *Int. J. Solids Struct.* **34**, 3041–3057.

Ding, H. J., Chi, Y. & Guo, F. 1999 Solutions for transversely isotropic piezoelectric infinite body, semi-finite body and bimaterial infinite body subjected to uniform ring loading and charge. *Int. J. Solids Struct.* **36**, 2613–2631.

Dunn, M. L. & Taya, M. 1993 An analysis of piezoelectric composite materials containing ellipsoidal inhomogeneities. *Proc. R. Soc. Lond.* A **443**, 265–287.

Dunn, M. L. & Wienecke, H. A. 1996 Green's functions for transversely isotropic piezoelectric solids. *Int. J. Solids Struct.* **33**, 4571–4581.

Dunn, M. L. & Wienecke, H. A. 1999 Half-space Green's functions for transversely isotropic piezoelectric solids. *J. Appl. Mech.* **66**, 675–679.

Eshelby, J. D. 1957 The determination of the elastic field of an ellipsoidal inclusion, and related problems. *Proc. R. Soc. Lond.* A **241**, 376–396.

Fan, H., Sze, K. Y. & Yang, W. 1996 Two-dimensional contact on a piezoelectric half-space. *Int. J. Solids Struct.* **33**, 1305–1315.

Faux, D. A. & Pearson, G. S. 2000 Green's tensors for anisotropic elasticity: application to quantum dots. *Phys. Rev.* B **62**, R4798–R4801.

Faux, D. A., Downes, J. R. & O'Reilly, E. P. 1996 A simple method for calculating strain distribution in quantum-wire structures. *J. Appl. Phys.* **80**, 2515–2517.

Faux, D. A., Downes, J. R. & O'Reilly, E. P. 1997 Analytic solutions for strain distribution in quantum-wire structures. *J. Appl. Phys.* **82**, 3754–3762.

Freund, L. B. 2000 The mechanics of electronic materials. *Int. J. Solids Struct.* **37**, 183–196.

Freund, L. B. & Gosling, T. J. 1995 Critical thickness for growth of strained quantum wires in substrate V-grooves. *Appl. Phys. Lett.* **66**, 2822–2824.

Gosling, T. J. & Willis, J. R. 1995 Mechanical stability and electronic properties of buried strained quantum wire arrays. *J. Appl. Phys.* **77**, 5601–5610.

Holy, V., Springholz, G., Pinczolits, M. & Bauer, G. 1999 Strain induced vertical and lateral correlations in quantum dot superlattices. *Phys. Rev. Lett.* **83**, 356–359.

Larkin, I. A., Davies, J. H., Long, A. R. & Cusco, R. 1997 Theory of potential modulation in lateral surface superlattices. II. Piezoelectric effect. *Phys. Rev.* B **56**, 15 242–15 251.

Mindlin, R. D. 1936 Force at a point in the interior of a semi-infinite solid. *Physics* **7**, 195–202.

Mohammad, S. N. & Morkoc, H. 1996 Progress and prospects of group-III nitride semiconductors. *Prog. Quant. Electron.* **20**, 361–525.

Mura, T. 1987 *Micromechanics of defects in solids*, 2nd revised edn. Kluwer.

Pan, E. 1997 A general boundary element analysis of 2-D linear elastic fracture mechanics. *Int. J. Fracture* **88**, 41–59.

Pan, E. 1999 A BEM analysis of fracture mechanics in 2D anisotropic piezoelectric solids. *Engng Analysis Bound. Elem.* **23**, 67–76.

Pan, E. 2002*a* Three-dimensional Green's functions in anisotropic magneto-electro-elastic bimaterials. *J. Appl. Math. Phys.* (In the press.)

Pan, E. 2002*b* Three-dimensional Green's functions in anisotropic half space with general boundary conditions. (Submitted.)

Pan, E. & Tonon, F. 2000 Three-dimensional Green's functions in anisotropic piezoelectric solids. *Int. J. Solids Struct.* **37**, 943–958.

Pan, E. & Yuan, F. G. 2000 Three-dimensional Green's functions in anisotropic piezoelectric bimaterials. *Int. J. Engng Sci.* **38**, 1939–1960.

Park, S. & Chuang, S. 1998 Piezoelectric effects on electrical and optical properties of wurtzite GaN/AlGaN quantum well lasers. *Appl. Phys. Lett.* **72**, 3103–3105.

Pearson, G. S. & Faux, D. A. 2000 Analytical solutions for strain in pyramidal quantum dots. *J. Appl. Phys.* **88**, 730–736.

Ru, C. Q. 1999 Analytic solution for Eshelby's problem of an inclusion of arbitrary shape in a plane or half-plane. *J. Appl. Mech.* **66**, 315–322.

Ru, C. Q. 2000 Eshelby's problem for two-dimensional piezoelectric inclusions of arbitrary shape. *Proc. R. Soc. Lond.* A **456**, 1051–1068.

Ru, C. Q. 2001 Two-dimensional Eshelby problem for two bonded piezoelectric half-planes. *Proc. R. Soc. Lond.* A **457**, 865–883.

Suo, Z., Kuo, C. M., Barnett, D. M. & Willis, J. R. 1992 Fracture mechanics for piezoelectric ceramics. *J. Mech. Phys. Solids* **40**, 739–765.

Tiersten, H. F. 1969 *Linear piezoelectric plate vibrations*. New York: Plenum.

Ting, T. C. T. 1996 *Anisotropic elasticity*. Oxford University Press.

Ting, T. C. T. 2000 Recent developments in anisotropic elasticity. *Int. J. Solids Struct.* **37**, 401–409.

Walker, K. P. 1993 Fourier integral representation of the Green's function for an anisotropic elastic half-space. *Proc. R. Soc. Lond.* A **443**, 367–389.

Willis, J. R. 1966 Hertzian contact of anisotropic bodies. *J. Mech. Phys. Solids* **14**, 163–176.

Wright, A. F. 1997 Elastic properties of zinc-blende and wurtzite AlN, GaN, and InN. *J. Appl. Phys.* **82**, 2833–2839.